Southern Plains Transportation Center
CYCLE 1

FINAL REPORT

2023–2024

USDOT BIL Regional UTC
Region 6

Surface Penetration and Imaging for Infrastructure Inspection using Radar Sensors as UAS Payload

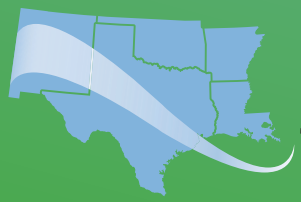

SOUTHERN PLAINS
TRANSPORTATION CENTER

Disclaimer

The contents of this report reflect the views of the authors, who are responsible for the facts and accuracy of the information presented herein. This document is disseminated under the sponsorship of the Department of Transportation University Transportation Centers Program, in the interest of information exchange. The U.S. Government assumes no liability for the contents or use thereof.

Technical Report Documentation Page

1. Report No. 69A3552348306	**2. Government Accession No.** [Leave blank]	**3. Recipient's Catalog No.** [Leave blank]
4. Title and Subtitle SURFACE PENETRATION AND IMAGING FOR INFRASTRUCTURE INSPECTION USING RADAR SENSORS AS UAS PAYLOAD		**5. Report Date** January 15, 2025 **6. Performing Organization Code** [Code]
7. Author(s) Yan (Rockee) Zhang Hernan Suarez Jorge Luis Alva Alarcon		**8. Performing Organization Report No.** [Report No.]
9. Performing Organization Name and Address Intelligent Aerospace Radar and Radio Team University of Oklahoma 3190 Monitor Ave Norman, OK, 73019		**10. Work Unit No. (TRAIS)** [Leave blank] **11. Contract or Grant No.** 69A3552348306
12. Sponsoring Agency Name and Address Southern Plains Transportation Center 202 West Boyd St., Room 213B The University of Oklahoma Norman, OK 73019		**13. Type of Report and Period Covered** Final Report: Sep 2023 to Jan 2025 **14. Sponsoring Agency Code** [Leave blank]
15. Supplementary Notes Conducted in cooperation with the U.S. Department of Transportation as a part of the University Transportation Center (UTC) program.		
16. Abstract The project develops a novel wideband, small-sized and super-lightweight radar payload for general small Unmanned Aerial System (UAV), as a replacement of the traditional ground-penetration radar (GPR) for a broad range of infrastructure inspections, such as bridges, roads, pavements, and other concrete structures. The Year One work has been focused on the requirement analysis, feasibility study, simulation modeling and laboratory testing of specific prototype radar module based on the impulse radar concepts.		
17. Key Words Radar, UAS, bridge inspection, infrastructure inspection	**18. Distribution Statement** No restrictions. This publication is available at www.sptc.org and from the NTIS.	
19. Security Classification (of this report) Unclassified	**20. Security Classification (of this page)** Unclassified	**21. No. of Pages** 39 / **22. Price** N/A

Form DOT F 1700.7 (8-72) Reproduction of completed page authorized

SURFACE PENETRATION AND IMAGING FOR INFRASTRUCTURE INSPECTION USING RADAR SENSORS AS UAS PAYLOAD

FINAL REPORT
SPTC Project Number: CY1-OU-02

Submitted by
Dr. YAN (ROCKEE) ZHANG (PI)
Dr. Hernan Suarez (Co-PI)
Jorge Luis Alva Alarcon (Graduate Student)
School of Electrical and Computer Engineering (ECE) and
School of Civil Engineering and Environmental Science (CEES)
The University of Oklahoma

Prepared for
Southern Plains Transportation Center
The University of Oklahoma
Norman, OK

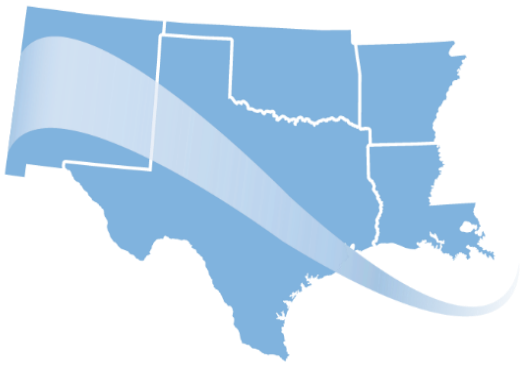

SOUTHERN PLAINS
TRANSPORTATION CENTER

January 2025

Acknowledgments

The project team appreciates the support and guidance from all staff members at the Southern Plain Transportation Center (SPTC), especially Dr Musharraf Zaman and Royce Floyd, as well as the support and advice from USDOT collaborators.

Table of Contents

List of Figures

List of Abbreviations and Acronyms

DOT .....Department of Transportation

FHWA .....Federal Highway Administration

FDTD.....Finite-Difference Time-Domain

GPR.....Ground Penetration Radar

NTL .....National Transportation Library

ROSAP .....Repository & Open Science Access Portal

RF .....Radio Frequency

SDR.....Software-defined Radio

UAV .....Unmanned Aerial Vehicle

UAS.....Unmanned Aerial System

UGV .....Unmanned Ground Vehicles

UWB .....Ultra-Wideband

UWBR.....Ultra-Wideband Radar

Executive Summary

This project addressed the initial challenge and feasibility analysis of using ultra-wideband impulse radar (IR) and lower-frequency band frequency sweeping radar as Unmanned Aerial System/Vehicle (UAS/V) payload for the missions of infrastructure inspections. The infrastructure includes bridges, roads, pavement surfaces, and other transportation structures. The OU-IART team has completed the planned tasks and milestones as shown in the following list:

Task 1: (100% Complete)

Detailed requirement analysis (Description: Consult with the project stakeholders regarding related engineering standards. The outcome will confirm the requirement documents about sensor performance, frequency range, size, weight and power, and imaging capability. Outcome: Documentation and report summarizing the near- and long-term needs from the infrastructure inspections.)

Task 2: (100% Complete):

Sensor system designs and lab verifications (Description: A detailed engineering design based on existing prototypes, determining the tradeoffs based on the state-of-the-art components and cost targets, and evaluating an option based on software-defined radio (SDR). Outcome: An initial prototype radar sensor design suitable for UAS deployment with initial lab test data.) The team improved the 7.3 GHz sensor packaging for lab tests and measurements. We continue experimenting with different antenna versions for this design and further enhance the reliability of the radio frequency (RF) signal path. For the L-band sensor design, we have started testing the signal source in the lab based on the tracker signal generator and identified a digital-scope-based receiver option. This simplified design does not cost much money but can give us some good initial verifications.

Task 3: (100% Complete):

Modeling and Simulation. (Evaluate radar signal penetration and propagation model for different types of Bridge, road, and construction materials. The model will further refine the radar sensor configuration design and tuning. Outcome: Documented and published simulation model containing the data analysis to guide further engineering designs.) Year One studies has established simulations and measurements using the initial lab setup—pending measurements using the actual concrete blocks. The team found many improvements in the simulation models and processing steps for crack detection. More details of this progress will be discussed in depth in the publications.

Task 4: (100% Complete):

Initial UAS payload design and verification. (Initial mechanical and electrical designs. The outcome will be mechanical drawings and further details on how the radar sensors would be installed into the UAV and any additional improvements needed based on the initial payload designs. Outcome: Drawing and data from the initial payload design and mechanical verification.) The team improved and analyzed the UAV payload designs for this period. Some interesting studies have been conducted on the interactions between the UAV onboard radio and the radar sensor, and so far, no problems have been found.

1. Introduction

The project aims to improve the automatic inspection capability of infrastructure under all weather conditions. The specific objectives include: (1) Develop and demonstrate a new low-size, weight, and power radar sensor that meets the unmanned aerial system (UAS) payload requirements and the need for surface penetration inspections; (2) Establish a formal operational procedure that can be applied to the regional and national tasks; (3) Evaluate the performance and capability of an integrated UAS system and sensing payload through data collections under different environments; and (4) Achieve dual-function (imaging and profiling) through existing signal processing and applying novel machine-learning methods. The solution brought up significant benefits compared to state-of-the-art: (1) Capability of inspecting underneath structure anomalies and problems; (2) Capability of penetrating the surface coverage such as dirt, rain, snow, or ice for examination of structure below; (3) Capability of operation near or within adverse weather and climate conditions, where the infrastructure assets are mostly in danger; and (4) Either using radar alone or in combination with cameras, the proposed sensor package would provide a reliable solution for surface structure inspection and potentially below-surface non-destructive testing and examination from a standoff distance, under all-weather conditions, such as snow and dust coverage.

The team executed a progressive engineering approach based on existing wideband, lightweight radar technology and improved the system and design for more challenging infrastructure inspections. This research was conducted through four tasks. Task 1 involves a detailed requirement analysis. In this task, the research team worked with the project stakeholders and consulted with the related engineering standards to perform a thorough requirement analysis. The outcome was confirmed requirement documents about sensor performance, frequency range, size, weight and power, and imaging capability. Task 2 involved sensor system designs and lab verifications. The research team performed a detailed engineering design based on existing prototypes, determined the tradeoffs based on the state-of-the-art components and cost targets, and evaluated an option based on a software-defined radio (SDR). Task 3 involved modeling and simulation. The research team assessed radar signal penetration and propagation models for different types of bridge, road, and construction materials. The model further refined the radar sensor configuration design and tuning. Task 4 included initial UAS payload design and verification, including mechanical and electrical designs based on the IF1200A UAS and its payload requirements for the radar design. The outcome was mechanical drawings and further details on how the radar sensors would be installed into the UAS, and additional improvements needed based on the initial payload designs.

2. Literature Review

Even though radar technologies, such as ground penetration radar (GPR) and synthetic aperture radars (SAR), have been investigated extensively in the previous USDOT projects [1-2, 7, 9, 11, 15-17, 19-20, 22, 24, 27-30], based on the advantages of all-weather and surface penetration sensing capabilities, a small, agile, and low-power version of such radar as a payload of unmanned aerial vehicle (UAV) or unmanned ground vehicles (UGV) have not yet been demonstrated before. Another significant trend in bridge/road/pavement inspection is robot-based, automatic, multi-sensor integration from a distributed network [13, 21-24, 29]. Several manned ground-based platforms with cameras and other sensors (LIDAR, acoustic, piezoelectric, IR, RFID, etc.) have been reported before from DOT projects [3-6, 10, 12-13, 14, 16, 18, 25-26, 31]. This includes machine learning (ML) processing methods to identify structure and material health issues better [4, 9, 32-33]. However, more in-depth investigation is still needed to mature these algorithms. Transferring these R&D efforts to operational capabilities still depends on real-world challenges such as infrastructure accessibility, safety, environments, and maturity of the sensor systems. The novel contribution of the new radar sensor package proposed from this project mainly lies in three aspects: (1) Wideband microwave radar inspection with both designs from lower-frequency, traditional GPR frequency band, and higher frequency, microwave radar band that offers better resolution and smaller sensor aperture sizes, by leveraging the latest component technology of radar sensors. (2) Enabling and implementing the integration into a small UAS (sUAS) platform, which has fewer restrictions from ground traffic, can access the problematic areas for human operators and demonstrate such platforms through flight tests. (3) Introduction of machine learning (ML) method based on high-fidelity physical modeling of the interactions between structures and microwave sensors and decision-tree type sensor data models; thus, the capability of detecting various types of defects in the 3D domain is enhanced compared to existing radar sensors. However, compared to the state of the art listed above, the UAS-based radar payload faces significant new challenges. First, the standoff distance from the radar to the surface structure leads to a hybrid, heterogeneous propagation domain combination compared to the existing GPRs. Second, extreme size, weight, and power constraints prohibit installing or deploying traditional ground vehicle-based radars.

3. Materials and Methodologies

3.1 Sensor System Requirements and Operational Concepts

We first reviewed the literature and current standards for bridge inspections and instruments. We are currently focusing on UAS deployment solutions and scenarios. Some of these analyses are depicted in the following Figure 1. In this output, we summarized the initial literature analysis of the bridge inspection practice. We identified the key aspects of interception between existing practices and the capabilities of UAS-carried sensor systems. These initial operational scenario concepts are depicted in Figure 1. Also, we started the revised radar sensor design based on an existing preliminary ultra-wideband (UWB) impulse radar design, with the current estimation of the size-weight of the radar PCB board marked in Figure 1 as well.

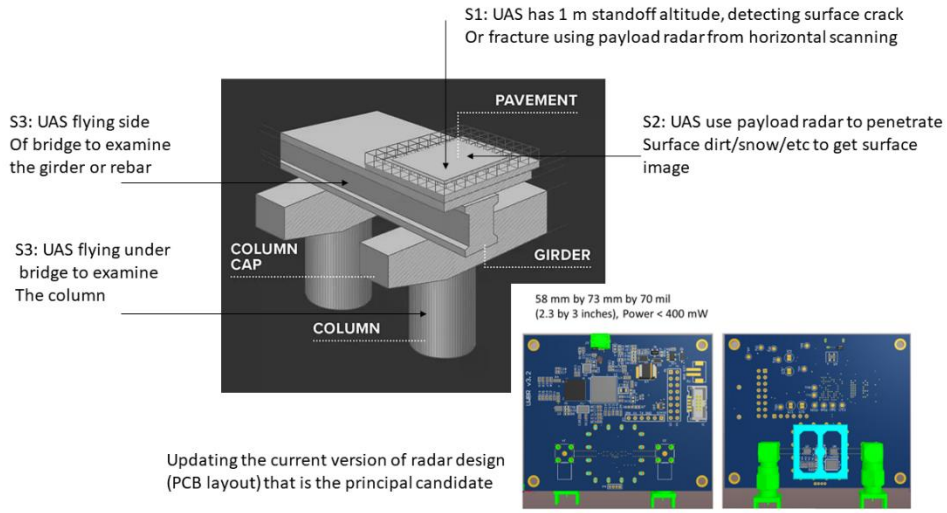

Figure 1: Radar-based operational concept and core hardware for the ultra-wideband impulse radar design option.

Updated requirement studies for UAS-based bridge inspection using the wideband radar payload and the initial estimation of radar core-board size/power based on one of the existing designs. The basic modeling of the UAS-mounted sensor (Task 3 and Figure 2) summarizes the radar sensing modeling of the multi-layer materials. A preliminary analytical model was established and utilized to calculate the initial radar imaging performance.

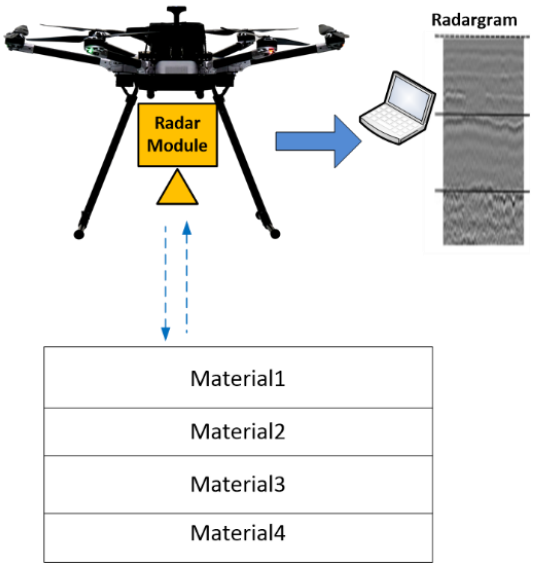

Figure 2: The proposed long-term goal and UAS payload requirement include estimating the material type and depth of each layer in the structure (such as pavement) and detecting faults/anomalies in the structure using A/B scan patterns like the existing GPRs.

3.2 Radar Sensing Mechanism and Modeling Basis

The radar was mounted on a drone to perform continuous scans. Data was collected and pre-processed in the module and then transferred to a computer for further processing. Figure 3 shows the "roadmap" of the UWB radar sensor development, for which we have been focused on the "Analysis" and "Modeling-Simulation" subtasks.

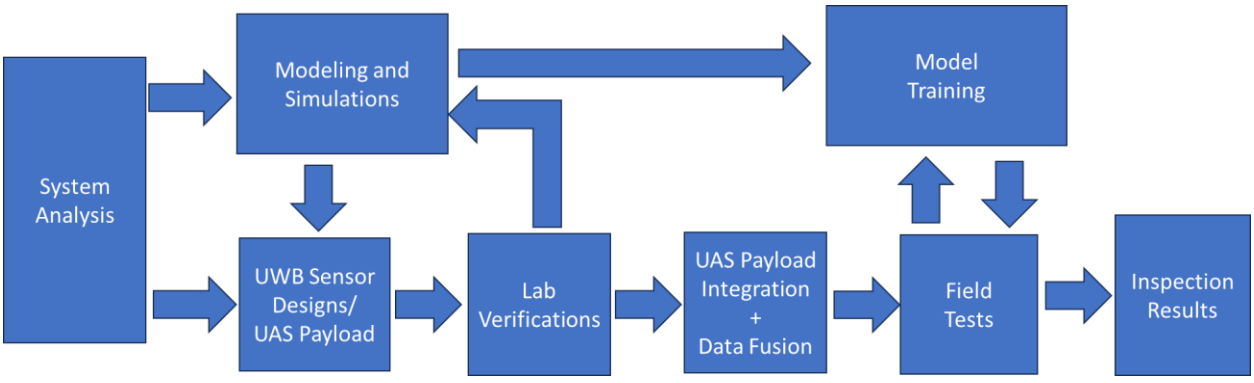

Figure 3: The flow diagram represents the key processes for implementing our radar sensor system.

3.3 Design and Deployment of Radar Sensors

3.3.1 Impulse Radar Sensor: Theory and Design Method

An impulse radar is a type of ultra-wideband radar that uses a burst of short pulses to achieve the wide signal bandwidth. Figure 4 depicts the measured transmit signal from our impulse radar in the time domain (left) and the frequency domain (right). The figures also show the differences between the two operational frequency bands (7.29 GHz and 8.7 GHz).

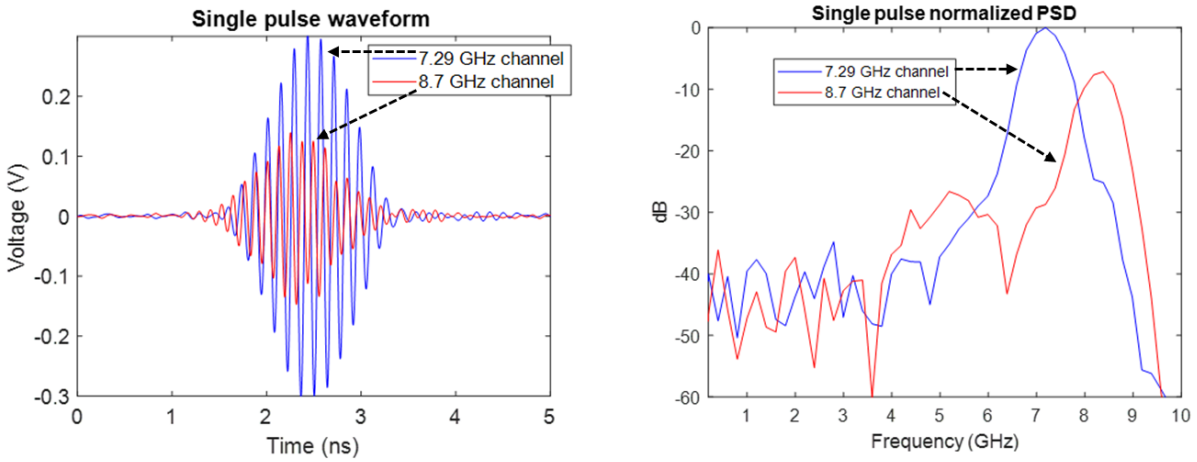

Figure 4. Time-domain and frequency-domain characteristics of UWB waveforms

The impulse signals, when propagating through the ground medium such as concrete, asphalt and soil, would show unique signatures in the radar return signals. One of the examples are shown in Figure 5 as below. The structure in this example is a concrete block containing multiple inner layers along the radar range direction. Based on this phenomenon, the system can be designed to detect and identify the anomalies inside the structure such as cracks and delamination.

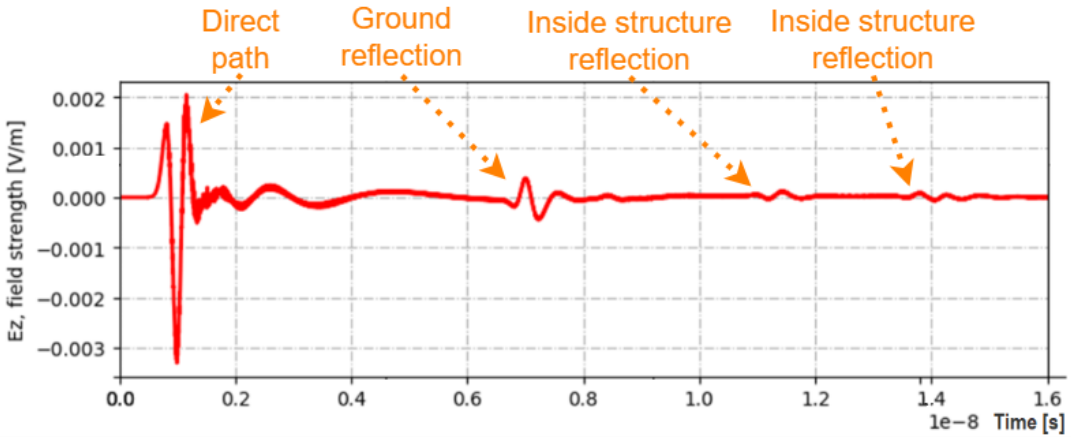

Figure 5. Propagation behavior of impulse signals in the typical ground structure.

3.3.2 Software-Defined, Lower-Frequency Penetration Radar Design Method

As part of the effort to combine the electronic scanning capability at X-band with both narrow-band and wide-band probing capabilities, various design options with evaluation hardware were employed. The current UWB radar PCBs operate at either 7.3 or 8.75 GHz. These frequencies provide high-resolution radargrams but offer significantly lower penetration depths. Given this, research in L-S-band radars with 1 – 4 GHz operating frequencies was also initiated. L – S-band radars offer improved propagation characteristics, leading to increased penetration depths. However, lower frequencies, as in the case of L-band radars, hinder the resolution of the produced radargrams, reducing the likelihood of detecting miniature deformations in concrete structures. Research with the educational tool ADALM-PLUTO, an open-source SDR with programmable operating frequencies in the UHF, L, and S microwave bands, has offered insight into solutions with lower frequencies. Temporary research is being conducted with Pluto and the Analog Devices CN0566 Phased Array kit (Phaser) in target identification and transmission power calculations. A demonstration of target identification and distance determination is shown in Figure 6**.** Although the phased array utilizes a 10.25 GHz operating frequency, the frequency-adapting hardware employed by Phaser can be similarly implemented with the current UWB radar PCBs to obtain a lower output frequency of the GPR. Figure 7 illustrates a simplified hardware design diagram for adapting the 7.3 GHz output of the UWB radar to a more acceptable L- or S-band frequency through down-conversion.

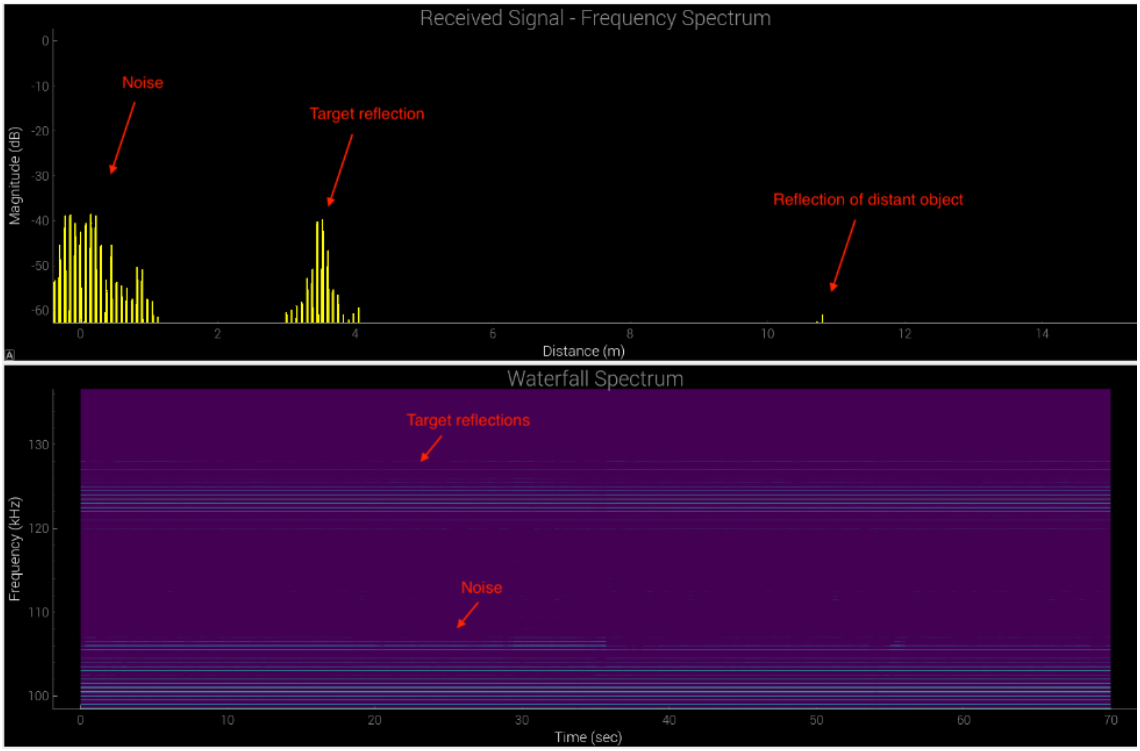

Figure 6. Examples of range and frequency responses of FMCW-based radar sensor

Frequency spectrum plot, converted to distance, of received signal reflections of target object placed at 3.75 m (top), waterfall spectrum of historically received signals over 30 seconds (bottom).

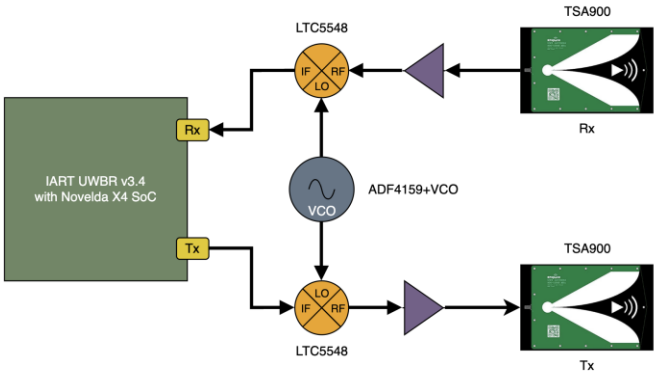

Figure 7. Examples of a design solution to adapt the UWB radar's 7.3 GHz frequency to an acceptable L or S band range.

The Year One project effort focused on matching simulation modeling with lab measurements, we also made some progress on designing and verifying the L-band penetration radar version based on the simple design, as shown in Figure 8. We tested the TG44A sweeping signal generator from the lab bench environment and verified the signal generation capabilities.

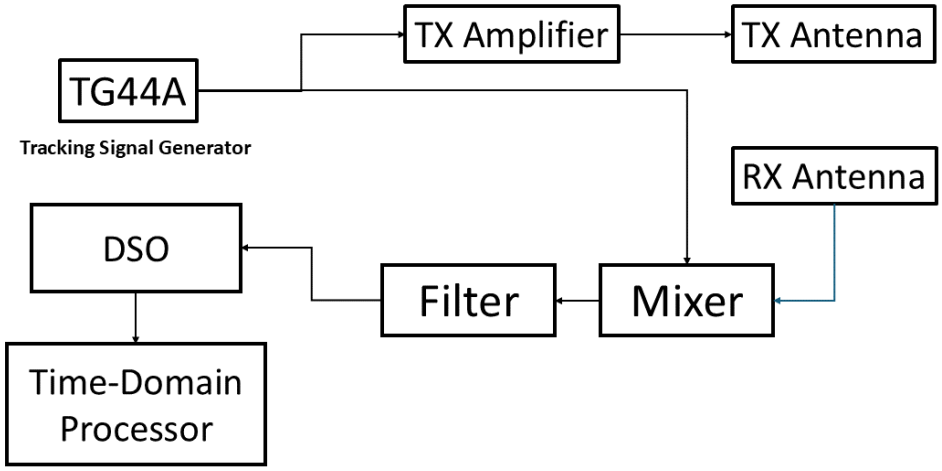

Figure 8: Design diagram of the L-band sensor prototype for initial lab test.

3.4 Modeling, Simulation, and Signal Processing

The characteristics of the UWB radar and the resulting achievable penetration depth were explored. A MATLAB program was developed that allowed the entry of standard medium constants of concrete, resulting in various calculated data. After researching and inputting concrete permittivity, permeability, and conductivity approximations, the program used these values to calculate the wave velocity, attenuation, skin depth, and probing distance of the GPR wave within concrete.

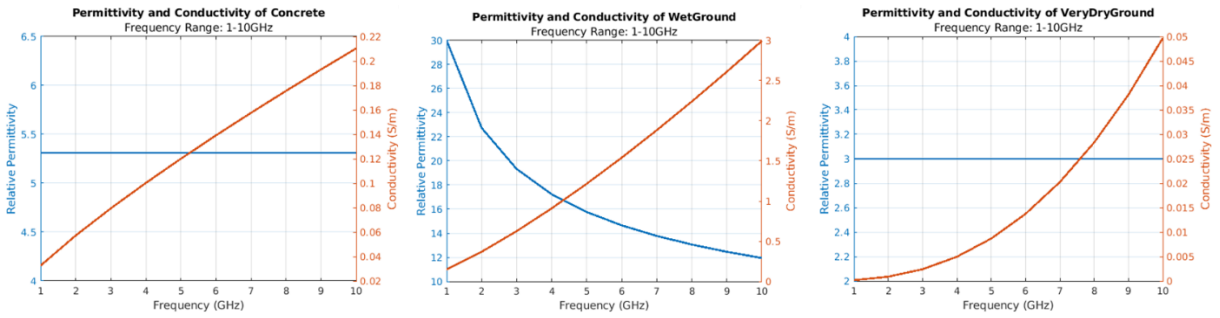

(a) **(b)** **(c)**

Figure 9: **Permittivity and Conductivity for (a) Concrete, (b) Wet-Ground, and (c) Very-Dry-Ground.**

Table 1: Modeling Calculations for Concrete: Using Wave Regime Approximation

Parameter	Value
Velocity of the wave	0.130189 m/ns
Attenuation of the wave	2.6664839 dB/m
The Skin Depth of the wave	0.374633 m
Skin Depth Check	0.375257 m
The Probing Distance of the Radar in the concrete	1.123898 m
Probing Distance check	1.123898 m

We also created a digital model of a sample piece of a bridge structure. Given the broad possibilities for these models, we created a three-layer model that incorporates air, asphalt, and concrete. Within the concrete layer, we added an air gap layer (first attempt at cracking detection) and three cylinders representing rebars. The software used is 'gprMax,' which is open-source software that simulates electromagnetic wave propagation using the Finite-Difference Time-Domain (FDTD) method. In Figure 10-11, the digital model can be seen.

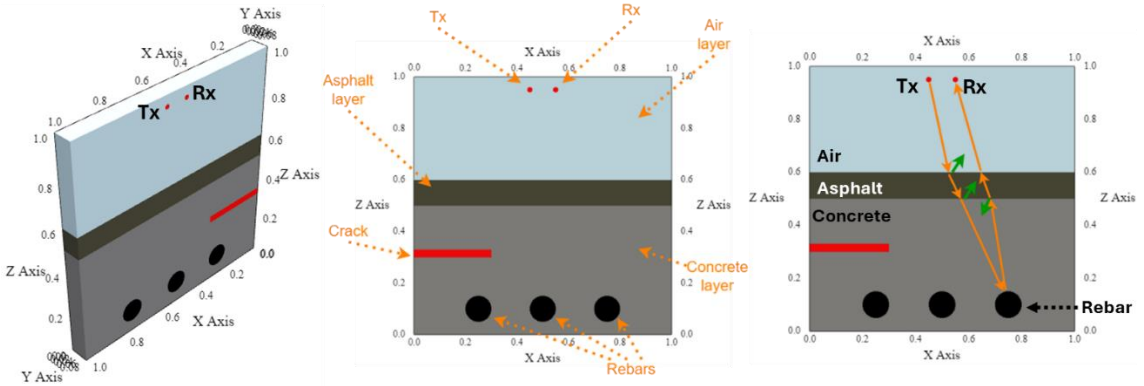

(a) (b) (c)

Figure 10: (a) GprMax initial model of a slide of a concrete bridge. (b) The model with its corresponding legend. (c) Example of one on the waves' reflections for the most top proper rebar inside the concrete.

The modeling and simulation of the UWB inspection sensor have progressed to a stage of detailed and more realistic modeling, with improved incorporation of antenna effects. The setup in Figure 11 now includes the realistic modeling of the TAS900 antennas (the first time precisely modeled in the GPRMax environment). The antenna was placed in different orientations, and the crack/defect was also set to various sizes and locations.

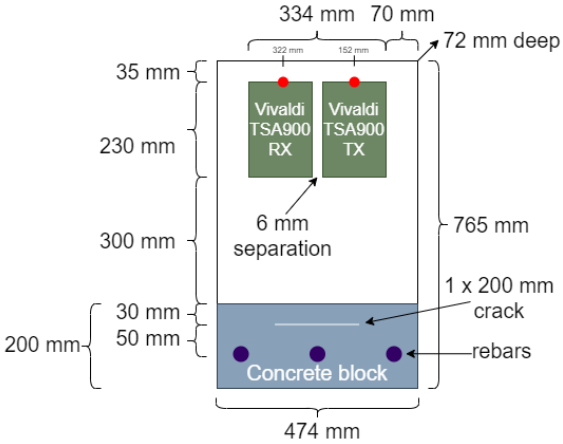

Figure 11: Example of improved simulation configuration and geometry.

One of the critical issues we addressed was the difference in the time-impulse responses of a realistic antenna versus an ideal antenna, which has infinite bandwidth and no port mismatching. Figures 12 and 13 illustrate this effect. When the material block has a complex internal structure or a tiny crack or defect, the time-impulse response of the antenna itself may overwhelm the "target" responses from multiple reflections.

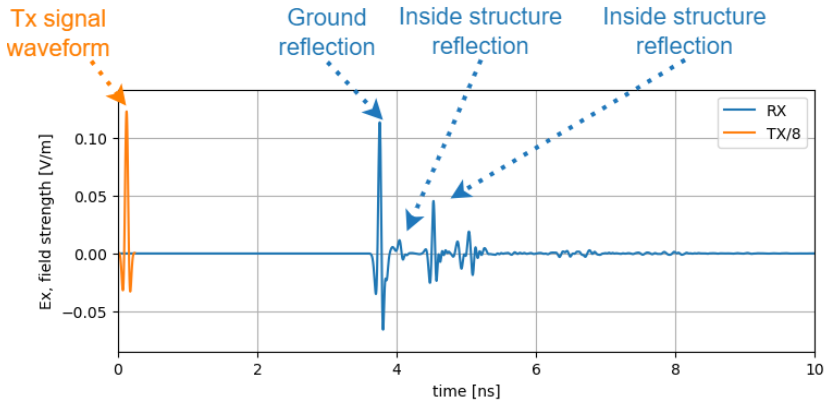

Figure 12: The receiver's E-field strength uses the ideal Hertzian Dipole when applying a Ricker function as the excitation waveform. A simple filter subtracts the non-obstacle signal.

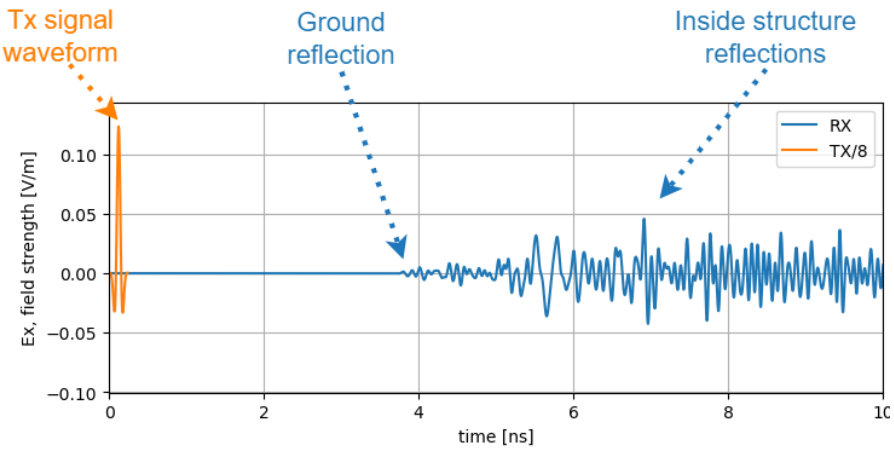

Figure 13: E-field strength in the receiver using the Vivaldi TSA900 when a Ricker function excitation waveform is applied. A simple filter by subtracting the non-obstacle signal is used.

The team developed during this phase of the project a solution that is based on a reference "signature template" to cancel out the multiple reflections. For this strategy, it was necessary to measure the echo from the impulse without any obstacle (this can be done inside an anechoic chamber). This information was then saved and used to compensate for the measured data. The following simulation results compare the values between a Hertzian Dipole (the reference) and the Vivaldi TSA900 antenna. The concrete was placed at 2.2 m, and the crack inside at 2.3 m. After applying the signature template, it was possible to reveal the distances of 2.21 m and 2.32 m for the concrete and the crack, respectively. Figure 14 shows the results after applying the signature template, and the distances for the concrete and the crack were able to be measured and detected.

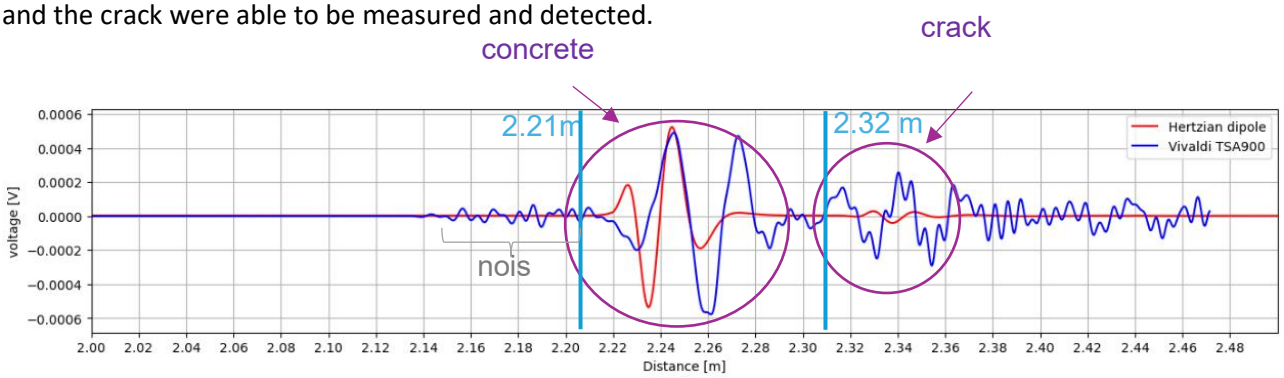

Figure 14: Comparison of the measured data using the Hertzian Dipole vs the Vivaldi TSA900 after applying the signature template strategy.

A novel algorithm was developed to process the time-domain range sampling returns and generate the A-Scan and B-Scan images. The details of these algorithms will first be published in the April 2025 SPIE DS conference presentation, while a more in-depth journal paper is being prepared.

3.5 Experiment Setup and Verifications

The initial test and implementation were focused on the laboratory test setup (Figure 15(a)) and the initial measurements of rebar and concrete specimens (as shown in **Figure 15(b)).** These are the necessary initial verifications of the radar sensor system. The test setup emulates the horizontal flight

scanning of UAVs by placing the radar and antennas on a downward-pointing rack structure. The vertical penetration measurement range is up to 10 meters.

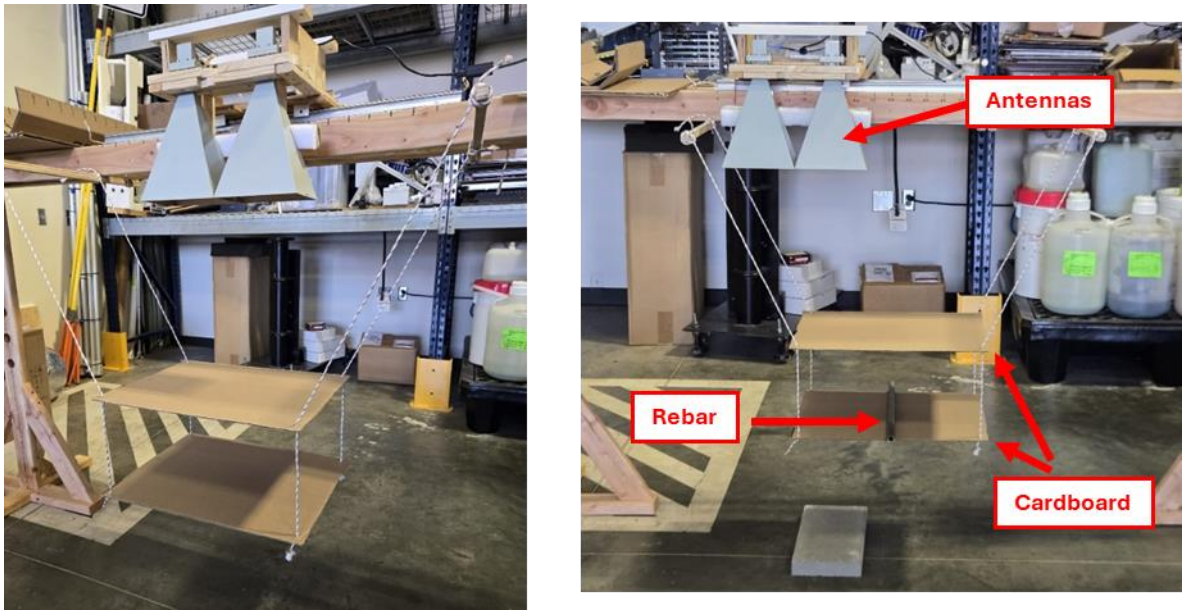

(a) (b)

Figure 15: Current lab-measurement setup/apparatus. (a) Using downward pointing standard horn antennas and suspended cardboard holders. (b) Initial mounting of rebar in the measurement setup.

The initial laboratory tests during the year one study aimed to emulate the vertical pointing measurements in a cluttered and realistic environment and test the essential interference/clutter cancellation solutions in both 1D (A-scan) and 2D (B-scan) signatures. Once it was confirmed that the measurements showed the expected results, the setup was taken to perform measurements with real concrete blocks.

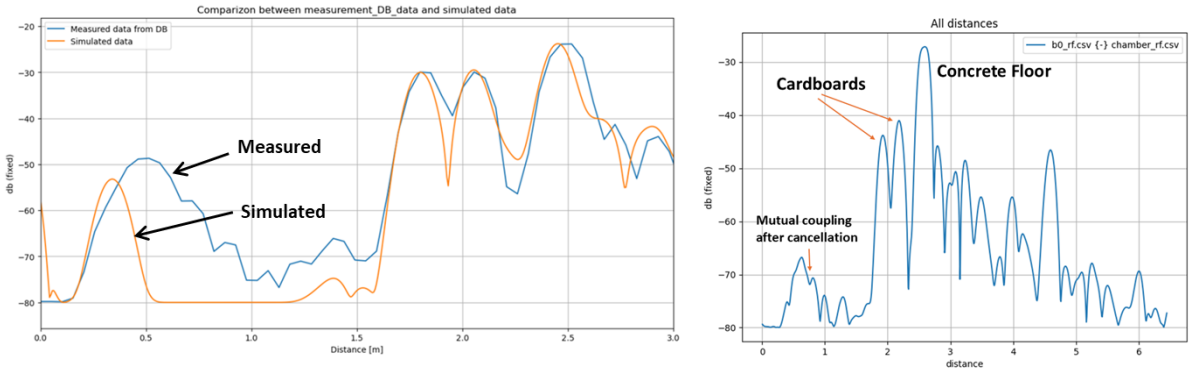

(a) **(b)**

Figure 16: (a) Comparison between simulated and measurement data when horn antennas are used for verifications. Vertical pointing with Figure 3(a) as the test setup. (b) 1D range profile after clutter subtraction, using Figure 3(b) as the test setup.

Figures 16 and 17 show the initial A-scan and B-scan data, respectively. In Figure 16(a), it can be observed that the cluttered environments with radar internal coupling interference can be reasonably

and accurately modeled using the FDTD-based EM simulation model described in Figure 1. The simple clutter background cancellation algorithm used the raw RF radar sample voltage and the clutter simulation/measurement "background" voltage samples, which yields about 17 dB clutter suppression improvement from the comparison between Figure 16(a) and (b). The insertion of the small brick and rebar samples were reliably detected from the 2D B-Scan result (Figure 17). Thus, the anomalies' resolution and size estimation capability are currently low, and no calibration was applied, but the initial results are encouraging. In the next step, we enhanced the horizontal resolution by applying coherent super-resolution processing and range calibrations.

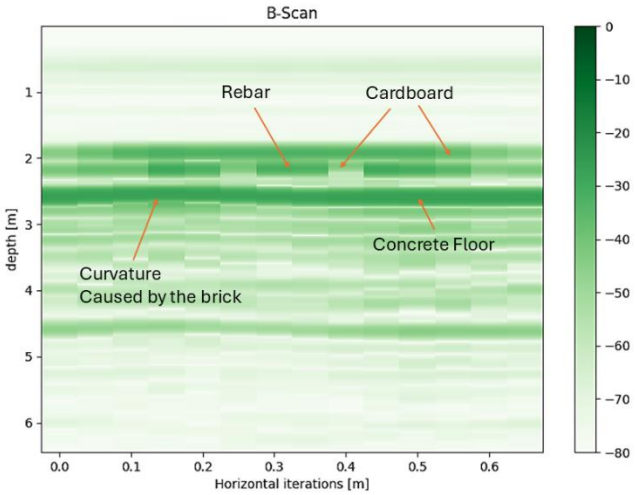

Figure 17: An example of the initial (uncalibrated) B-scan image of the rebar and other structures using the test setup in Figure 15(b). The imaging algorithm was rudimentary for this example.

The tests also compared the "clean" chamber environments with those in realistic outdoor environments, featuring roads and pavements, as shown in Figure 18. These tests verified that the noise patterns in these two environments were very similar, which helps us consider the need to stay within the chamber for the tests at all times, while there were additional clutter impacts from the road.

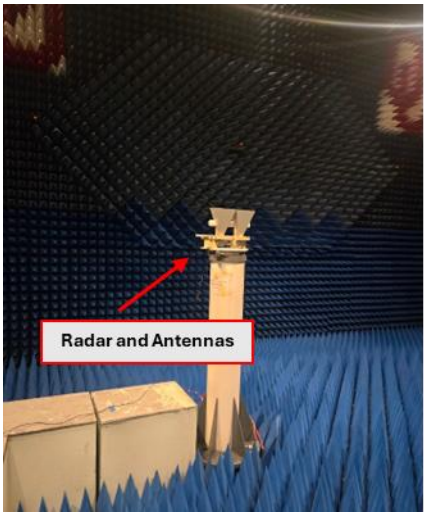

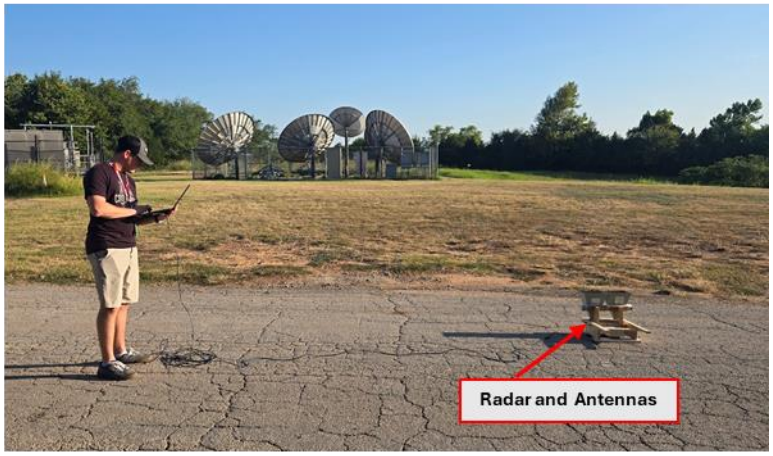

(a) **(b)**

Figure 18: Measuring noise pattern inside the chamber and outside the laboratory. (a) Antennas pointing toward the roof of the chamber (b) Antennas pointing toward the sky.

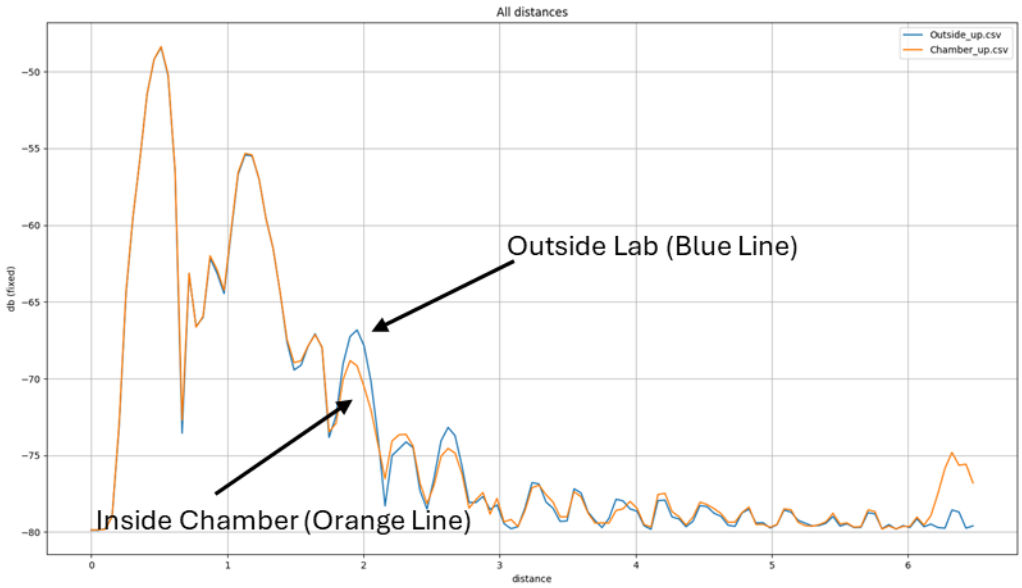

Figure 19: Comparison of range profiles (noise pattern) between pointing to the roof of the chamber and pointing to the sky (close to the pavement).

The Year One tests involved a concrete sample and a test fixture to guide the radar sensor. The fixture was constructed primarily of 2-by-4-inch timber to mitigate reflections of the radar signals. Using the concrete sample highlighted in Figure 20, identified with the help of and provided by the OU Fears Lab, allowed for controlled data collection using the current radar setup. The selected sample was ideal for testing as it was formerly used for bridge deck testing and experimentation. This offered the unique ability for initial data collection to be a moderately accurate representation of the data expected to be yielded from actual bridge deck samples. Furthermore, this sample offered multiple types of concrete with differing mediums, a rebar skeleton, and various crack sizes.

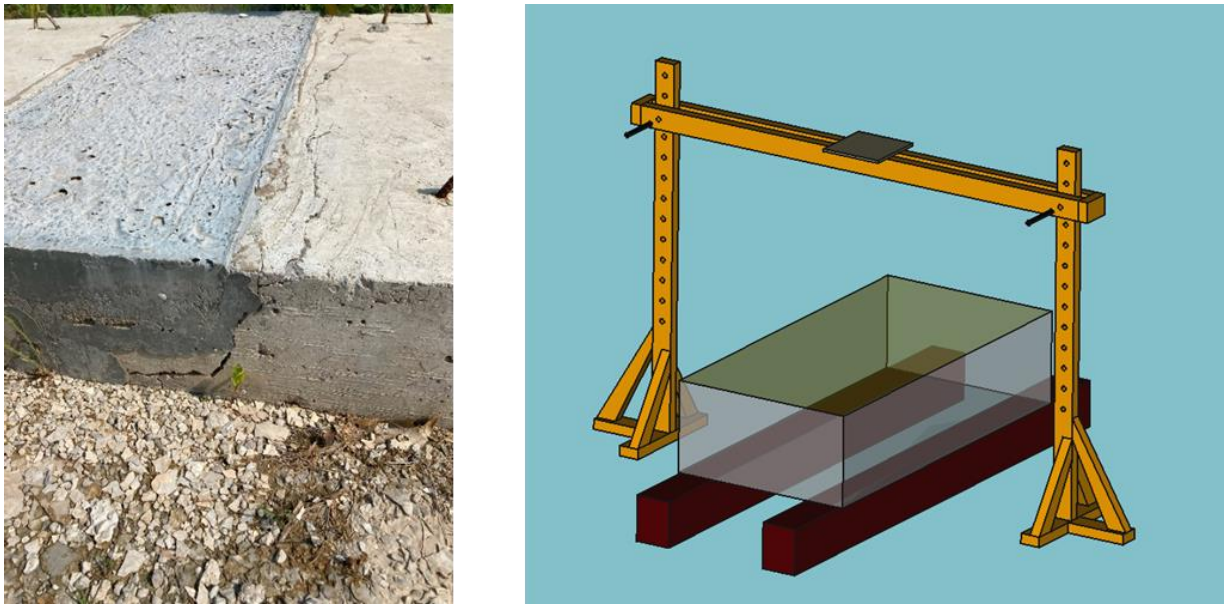

(a) (b)

Figure 20 (a) Sample concrete block with a crack, identified with help from the OU Fears Lab. (b) Test fixture design for mounting the concrete sample and radar for measurement data collection and verification.

The concrete sample was placed on wood supports to elevate it above the ground during the test, as shown in the outdoor test setup in Figure 21. This allowed conductive materials to be placed underneath the sample for radar detection. Raising the concrete offers a controlled environment for testing the penetration depths of the radar as well as the resolution qualities of different frequencies. Additionally, the test fixture enabled vertical translation of the radar to allow for data to be taken at varying heights from the surface of the concrete sample. By taking data at different heights, the maximum altitude of the drone from the sample can be determined based on the characterization of the data. Depending on the type of test, the desired radar for that test considered the equipment under test (EUT). The EUT was mounted to the square wood platform in the middle of the beam of the test fixture. Using custom mounting jigs, the antennas was mounted below this platform. Again, depending on the test, the antennas were determined based on the characteristics of the EUT. The antennas were mounted in such a way as to capture data in both the x and y-axes of the concrete sample. This offered a simple method to collect various data points for comparison. The EUT was directly connected to either a laptop or compact processing computer natively running the software code.

Figure 21 : Concrete block setup and measurement (OU-Fears Lab).

3.6 UAS Payload Design

As identified in previous reports, the ultrawideband radar (UWBR) board, version 3.4, featuring the UWB radar SoC, was the primary radar for data acquisition. The UWBR board offers a 7.3 GHz impulse for radar sensing. To protect the radar, it was placed in a customized sealed container, demonstrated in Figure 22, that offers ease of access to the electronics while providing versatile mounting solutions for the Inspired Flight (IF) IF1200A drone. The initial configuration consisted of an AC power supply unit and a compact processing computer mounted on the cargo rack of the IF1200A, the radar enclosure was mounted beneath this. The two ultra-wideband (UWB) Vivaldi TSA900 antennas were mounted to the cargo rails on either side of the payload.

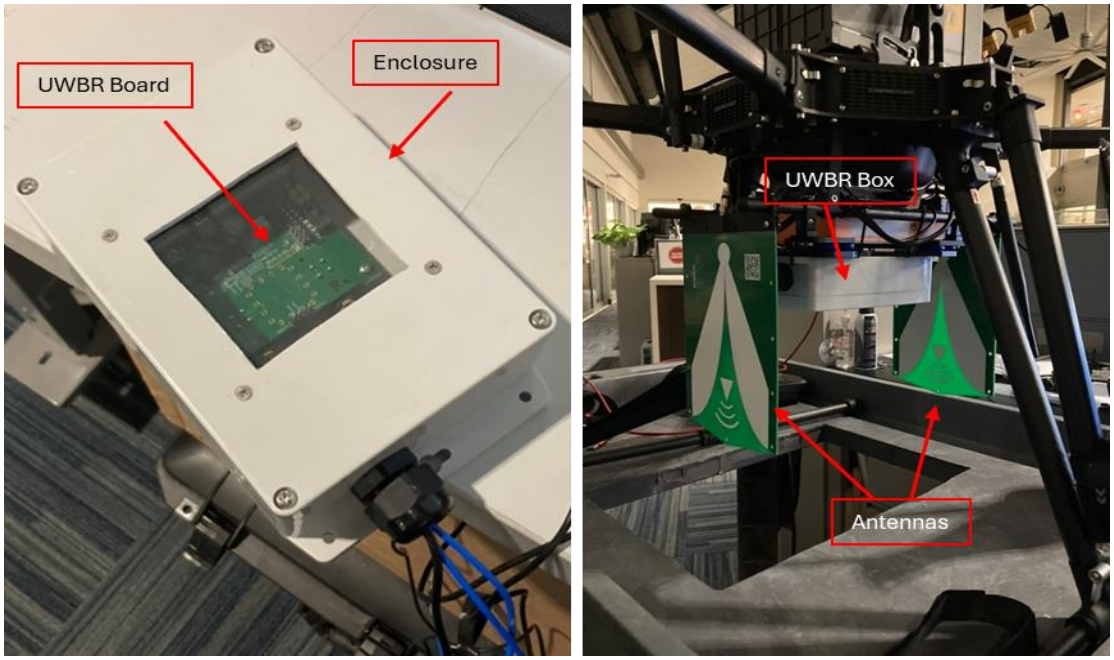

(a) (b)

Figure 22: (a) The UWBR board is placed inside the customized enclosure with a plexiglass window for LED debugging. (b) Initial mounting of the UWB radar board to the IF1200A drone with UWB TSA900 Vivaldi antennas placed on either side.

This configuration proved less than optimal after the initial radar-equipped test flight, as depicted in Figure 22(b). The scans showed significant peaks near the UAS during initial lab tests. It was then determined that this was caused by significant noise generated by the interference between the transmit (Tx) and receive (Rx) antennas. This initial setup is indicated in Figure 23.

Figure 23 : First test flight with the active integrated payload, taking samples of the road to ensure functionality.

After evaluating the noise causes, a new configuration was implemented to set the Tx and Rx antennas in the same plane. This helped mitigate the electromagnetic interference and antenna coupling experienced by the antennas due to their proximity. The radar enclosure was relocated to place the antennas in the same plane. The AC power supply unit and compact processing computer were moved farther away from the drone's center to accommodate the radar's new location. This allowed the TSA900s to be mounted directly underneath the cargo rack of the drone, as shown in Figure 24.

Figure 24 : The second payload configuration with TSA900 antennas in the same plane is mounted under the cargo rack, while the AC power supply and compact processing computer are mounted on the front of the cargo rack, with the radar enclosure placed directly behind.

The electromagnetic simulation illustrated in Figure 25 verified this new payload configuration. The simulation confirms the optimization of the new antenna mounting, considering the effect of the UAS airframe (i.e., landing legs). This is crucial as the UAS airframe is composed of carbon fiber, a highly conductive material that reflects electromagnetic waves, further producing noise peaks near the drone.

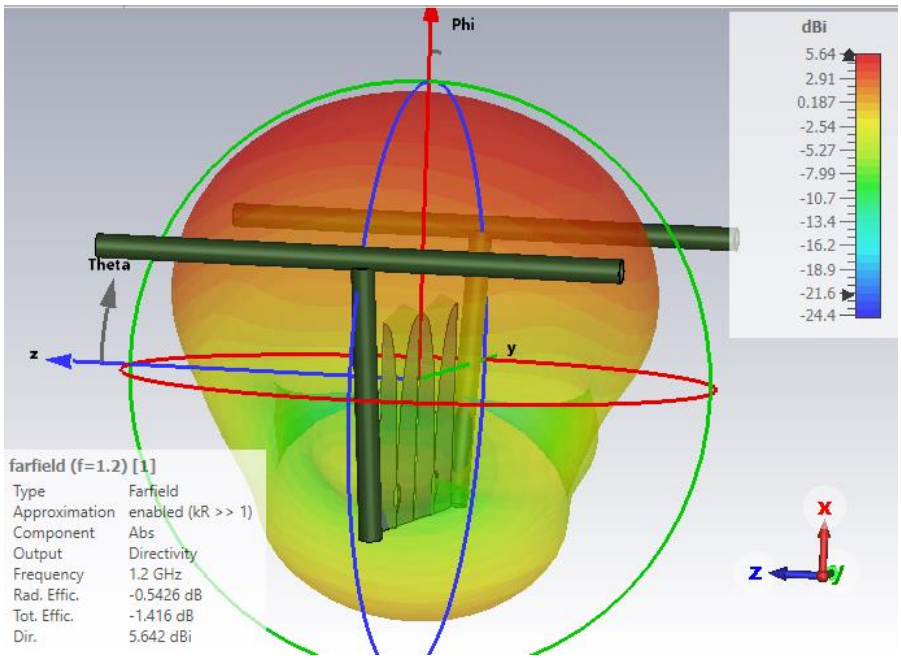

Figure 25: Simulation of the radiation pattern at the center frequency with the effects of the landing legs of UAS, which was used to guide the antenna placement optimization.

4. Results and Discussions

Although most of the current test and simulation results are presented in the previous sections, this section will highlight the system simulation (and limited measurement) results for the two-dimensional imaging mode (like the B-Scan imaging and detection of the traditional GPR). These important results show the feasibility of using the proposed radar sensor and hardware for the scanning pattern of UAS flight and payload data collection methods.

4.1 Simulation Scenarios

The Year One project's final simulation model utilizes scenarios that incorporate realistic antenna models, air-concrete material models, metal rebar models, and preliminary crack models in the structural regions. The simulation domain example, as shown in Figure 26, has an achieved domain size of 2 m by 2 m by 2 m, multiple metal rebars inserted in the concrete domain, and realistic models of both planar Vivaldi and standard horn antennas. Different types of realistic cracks in the concrete, as shown in Figure 27, are considered for modeling the cracking faults.

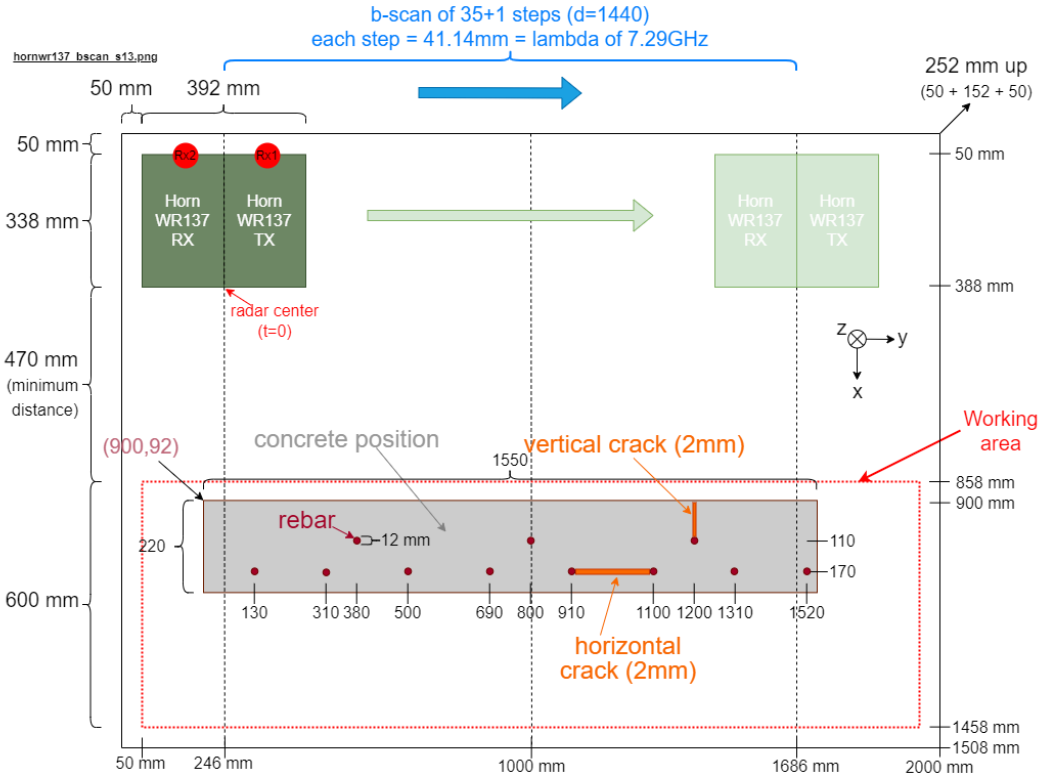

Figure 26: Simulation system geometry and structure setup.

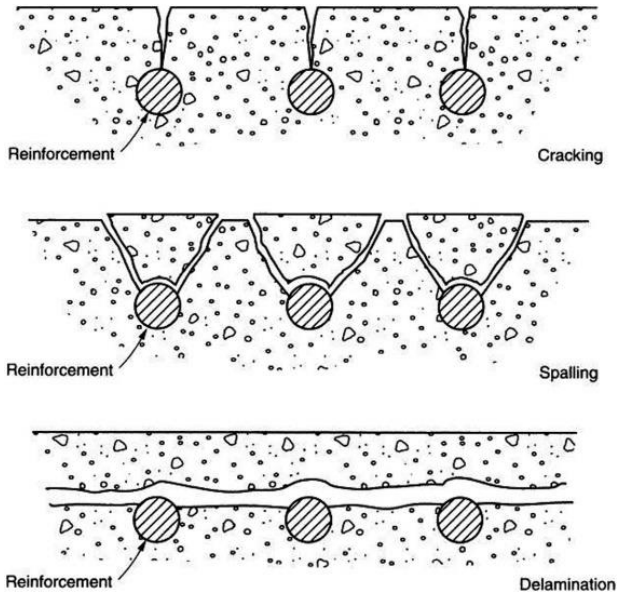

Figure 27: **Different types of cracks are considered in the simulation modeling studies. (https://highways.dot.gov/public-roads/autumn-2023/02)**

4.2 Typical Simulation Results and Initial SAR Image Formation

Based on the simulation scenario setup in Figure 26, we have successfully generated the A-Scan and B-Scan results with different configurations of rebars and cracks, as shown in Figures 28, 29, and 30. This simulation result is obtained by running the FDTD model on a server containing six GPUs. The impulse radar moved from left to right above the computational domain with horn antennas (transmit and receive) pointing downward, emulating the UAS flight trajectory. As shown in Figure 28's animations, the A-scan range profiles are collected and combined to apply a modified back-projection image formation algorithm. Figure 28 uses animation to show the image formation process. The results of the steps of this animation are shown in Figure 29, while in Figure 30 it is described the image processed shows a horizontal crack detected. In these cases, we can visually identify the image signatures of the concrete borders, the rebar structure, and the fault/crack.

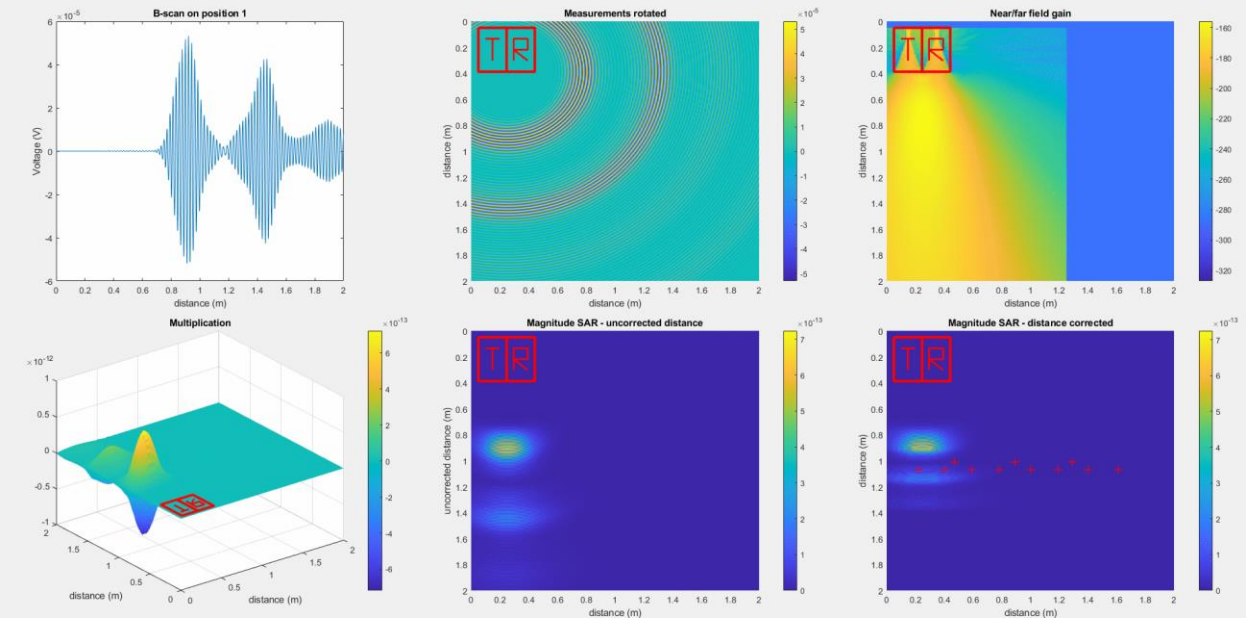

Figure 28: **UAS-based B-Scan image formation simulation with concrete domain setup.**

The system simulation model is still being developed and improved at this stage on these aspects: (1) A more efficient treatment of the hybrid domain setup and computation, which may contain air, water, concrete, asphalt, and other materials in the region, and need to be quickly re-configured to support a massive amount of simulation runs. (2) Improve image formation algorithms that can better utilize the time-domain delay and propagation information of UWB pulses at the near-fields. (3) Combining the physical model-based simulations, especially the antenna patterns, with the back projection algorithms for the imaging. (4) Applying machine-learning algorithms to detect cracks/faults from the resultant images.

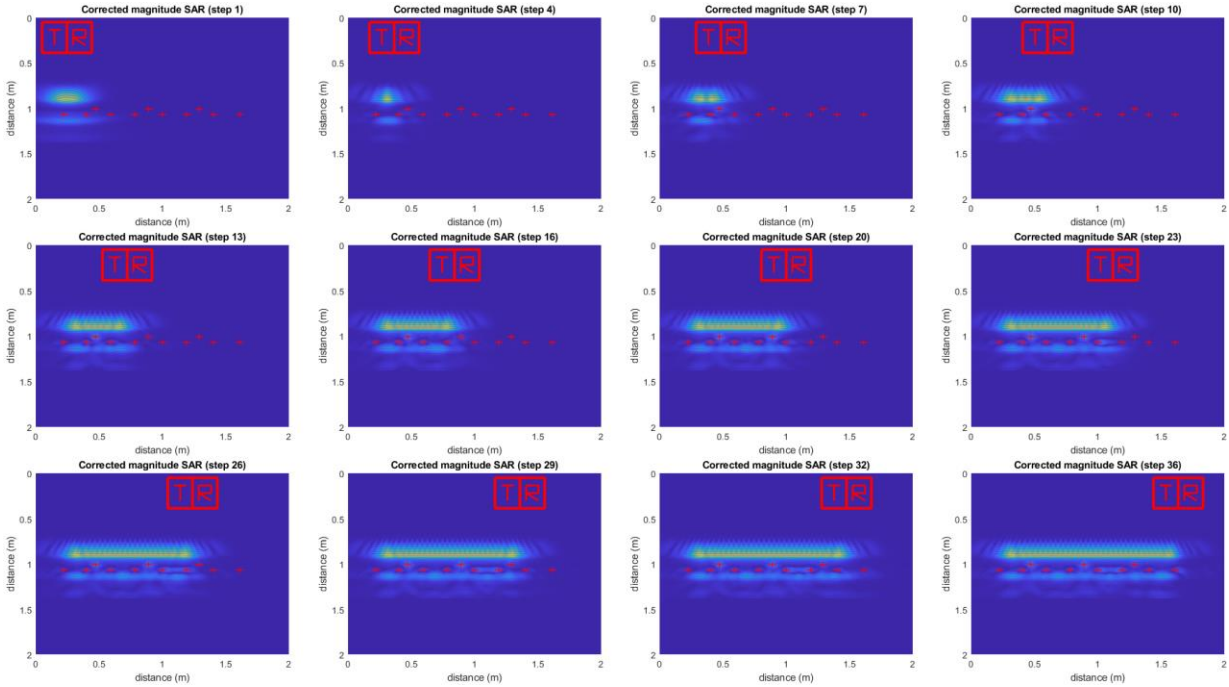

Figure 29: UAS-based B-Scan image formation simulation steps.

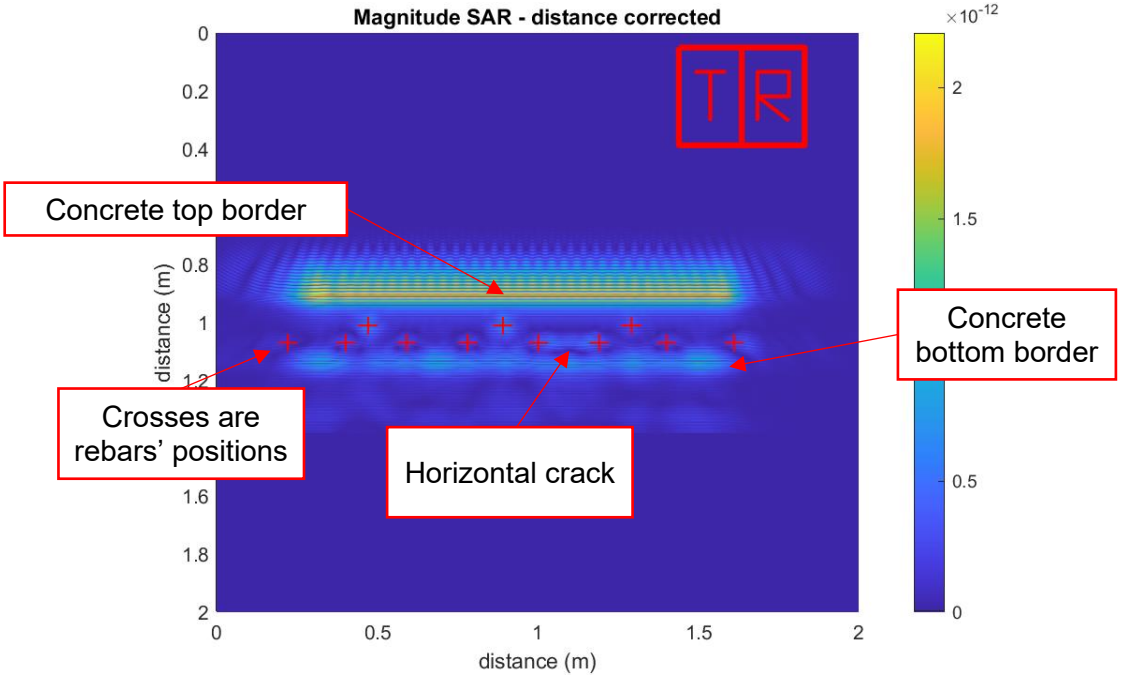

Figure 30: Result of the UAS-based B-Scan image formation simulation with concrete domain setup, a simulated "crack" structure is added between two rebars.

4.3 Preliminary Laboratory Measurement Results and Analysis

Figure 31 shows the initial image (with only stacking up of A-Scan processing instead of B-Scan processing) for the lab test configuration shown in Figure 21. Although this is highly rudimentary, one can identify the antenna mutual coupling at around 0.5 m, the small concrete block stacked on top of the larger one between 1-2 m distances, and numerous features below a depth of 2 meters. Figure 32 shows the output when the B-Scan image processing is applied, and focusing on the top concrete block can detect its width and depth of approximately 20x40cm. Once matured from simulations, more precise B-Scan algorithms will be applied here to obtain more features of the inner structures of the concrete blocks and the underneath features.

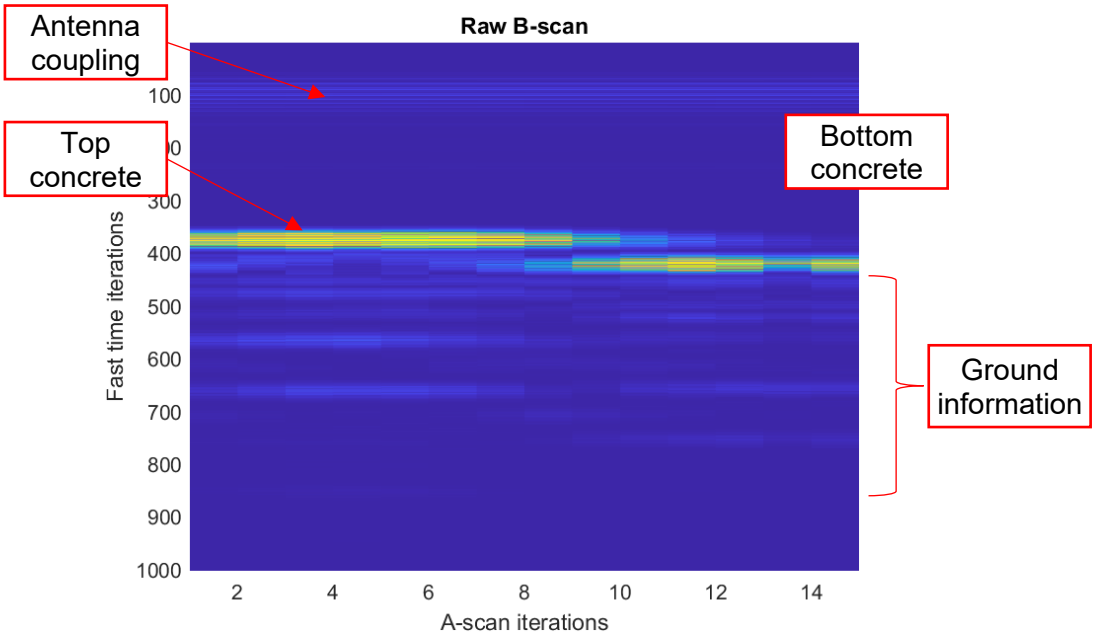

Figure 31: Initial B-Scan data recording from the FEARS Lab concrete block radar data collection and processing.

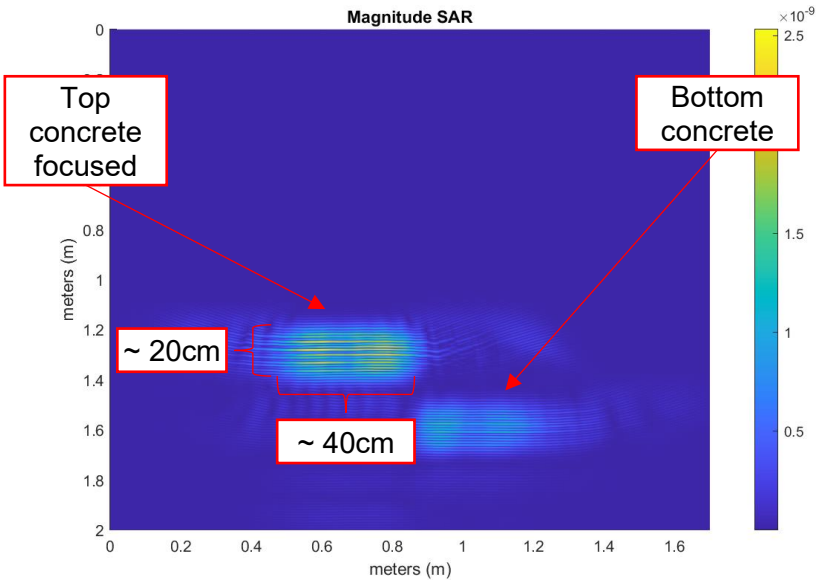

Figure 32: Image processing applied to the initial B-Scan data recording from the Fears Lab concrete block.

5. Conclusions and Recommendations

The completed Year One project tasks have reached the following conclusions:

(1) The feasibility of UAS-based UWB inspection radar operation is established through both simulations and initial laboratory measurements.
   - The usage of gprMax (FDTD solution tool) is critical for successful modeling tasks.
   - Importance of high fidelity, near-field responses of antenna models.

(2) Connection of physical propagation and scattering modeling (especially for the near-field modeling) with the SAR-type imaging processing algorithm is the key for the following step project tasks.

The next step of the project will continue to mature the related penetration radar technology and processing algorithms, testing them with more realistic scenarios, and verifying and demonstrating their capabilities.

6. Implementation of Project Outputs

During the Year One project period, the team held an initial discussion with the Choctaw Nation site (CNO) to explore further collaboration on the implementation. The latest point of contact is Marcus A Hartman (https://cnoaa.com/staff/marcus-hartman/). The CNO team is assisting in the investigation of a potential test site and scheduling.

7. Invention Disclosures and Patents, Publications, Presentations, Reports, Project Website, and Social Media Listings

A technical presentation was given on May 1st, 2024, for the DOT visit.

References

[1] Automated 3DGPR Analysis for Concrete Pavement Evaluation. [Project]. National Road Research Alliance. Start date: 16 Feb. 2024. https://rip.trb.org/view/2342073
[2] SPR-4839: Evaluation of Utilizing 3D GPR for Quality Assurance of Bridge Deck Rebar Cover and Delamination Screening. [Project]. Purdue University/Indiana Department of Transportation JHRP. Start date: 1 Sep. 2023. https://rip.trb.org/view/2253921
[3] Use of Distributed Acoustic Sensing (DAS) For Structural Health Monitoring of Asphalt Pavements. [Project]. Office of the Assistant Secretary for Research and Technology. Start date: 1 Oct. 2023. https://rip.trb.org/view/2291298
[4] Machine Learning Enabled Information Fusion of Heterogeneous Sensing for Infrastructure Monitoring (1.22). [Project]. Office of the Assistant Secretary for Research and Technology. Start date: 1 Oct. 2023. https://rip.trb.org/view/1996227
[5] Asset Characterization Using Automated Methods. [Project]. Missouri Department of Transportation. Start date: 1 Jun. 2023. https://rip.trb.org/view/2240243
[6] Bridge Element Deterioration for Midwest States. [Project]. Illinois Department of Transportation, Indiana Department of Transportation, Iowa Department of Transportation, Kansas Department of Transportation, Michigan Department of Transportation, Minnesota Department of Transportation, Nebraska Department of Transportation, North Dakota Department of Transportation, Ohio Department of Transportation, South Dakota Department of Transportation, Wisconsin Department of Transportation, Kentucky Transportation Cabinet. Start date: 6 Apr. 2023. https://rip.trb.org/view/1632303
[7] Air-Coupled GPR and HD Imaging for High-Speed Bridge Deck Evaluation. [Project]. Nebraska Department of Transportation. Start date: 1 Jul. 2022. https://rip.trb.org/view/1942637
[8] Detection and Monitoring of Material Aging and Structural Deterioration using Electromagnetic and Mechanical Sensors with Virtual Reality and Machine Learning Modeling (3.19). [Project]. Office of the Assistant Secretary for Research and Technology, Massachusetts Department of Transportation, University of Massachusetts Lowell. Start date: 1 Jun. 2022. https://rip.trb.org/view/1994582
[9] Integrate infrastructure performance monitoring using automatic crack evaluation system and convolutional neural network. [Project]. Office of the Assistant Secretary for Research and Technology. Start date: 1 Aug. 2021. https://rip.trb.org/view/1904953
[10] Development of a New Airborne Portable Sensing System to Investigate Bridge Response. [Project]. Office of the Assistant Secretary for Research and Technology. Start date: 11 Nov. 2020. https://rip.trb.org/view/1754671
[11] Advanced Sensing Technologies for Practical UAV-Based Condition Assessment (C20.2020). [Project]. Transportation Infrastructure Durability Center, Office of the Assistant Secretary for Research and Technology, University of Maine, Orono, University of Massachusetts Lowell, University of Vermont, Burlington. Start date: 1 Oct. 2020. https://rip.trb.org/view/1876108
[12] Automated Detection of Characterization of Cracks Using Structure-From-Motion Based Photogrammetry: A Feasibility Study. [Project]. Transportation Infrastructure Durability & Life Extension, Office of the Assistant Secretary for Research and Technology. Start date: 1 May. 2020. https://rip.trb.org/view/1742799
[13] Development of a System-Level Distributed Sensing Technique for Long-Term Monitoring of Concrete and Composite Bridges (C11.2019). [Project]. University Transportation Center Program, Transportation Infrastructure Durability Center, University of Massachusetts, Lowell, University of Vermont, Burlington, University of Maine, Orono, Office of the Assistant Secretary for Research and Technology. Start date: 1 Jan. 2020. https://rip.trb.org/view/1683657
[14] Bridge Cracks Monitoring: Detection, Measurement, and Comparison using Augmented Reality. [Project]. Office of the Assistant Secretary for Research and Technology. Start date: 1 Aug. 2020. https://rip.trb.org/view/1751167
[15] Integration of 3D Radar Technology into KYTC Operations. [Project]. Kentucky Transportation Cabinet. Start date: 1 Jul. 2019. https://rip.trb.org/view/1638642

[16] Reliability of Nondestructive Evaluation Methods for Bridge Decks. [Project]. Virginia Transportation Research Council. Start date: 11 Jun. 2019. https://rip.trb.org/view/1631580
[17] Electromagnetic Detection and Identification of Concrete Cracking in Highway Bridges (1.4). [Project]. University of Massachusetts Lowell, Office of the Assistant Secretary for Research and Technology. Start date: 1 Jan. 2019. https://rip.trb.org/view/1590550
[18] Condition Assessment of Corroded Prestressed Concrete Bridge Girders (C3.2018). [Project]. University of Massachusetts Lowell, Western New England University, Office of the Assistant Secretary for Research and Technology. Start date: 1 Jan. 2019. https://rip.trb.org/view/1591339
[19] RES2019-17: Concrete Bridge Deck Deterioration Assessment Using Ground Penetrating Radar. [Project]. Tennessee Department of Transportation, Federal Highway Administration. Start date: 1 Dec. 2018. https://rip.trb.org/view/1632584
[20] Deployment of Ground Penetrating Radar and Ultrasonic Tomographer Non-Destructive Techniques for Assessment of Corrosion-Deteriorated Adjacent Prestressed Concrete Box Beams. [Project]. Marshall University, Huntington, University of Virginia, Charlottesville, Office of the Assistant Secretary for Research and Technology. Start date: 1 May. 2017. https://rip.trb.org/view/1482474
[21] Climbing Robots with Automated Deployment of Sensors and NDE Devices for Steel Bridge Inspection (AS-2). [Project]. Office of the Assistant Secretary for Research and Technology. Start date: 1 Mar. 2017. https://rip.trb.org/view/1482661
[22] Autonomous Wall-climbing Robots for Inspection and Maintenance of Concrete Bridges (AS-3). [Project]. Office of the Assistant Secretary for Research and Technology. Start date: 1 Mar. 2017. https://rip.trb.org/view/1482671
[23] Quantitative Bridge Inspection Ratings Using Autonomous Robotic Systems (IM-2). [Project]. Office of the Assistant Secretary for Research and Technology. Start date: 1 Mar. 2017. https://rip.trb.org/view/1482754
[24] 3D Microwave Camera for Concrete Delamination and Steel Corrosion Detection (SN-4). [Project]. Office of the Assistant Secretary for Research and Technology. Start date: 1 Mar. 2017. https://rip.trb.org/view/1482775
[25] Battery-free Antenna Sensors for Strain and Crack Monitoring of Bridge Structures (SN-2). [Project]. Office of the Assistant Secretary for Research and Technology. Start date: 1 Mar. 2017. https://rip.trb.org/view/1482757
[26] Feasibility of Early Damage Detection Using Surface Mounted Sensors on Existing Pavements. [Project]. Department of Transportation. Start date: 1 Oct. 2014. https://rip.trb.org/view/1330247
[27] Analysis of Bridge Deck Smoothness vs. In-Place Geometry of Deck Reinforcement. [Project]. Research and Innovative Technology Administration. Start date: 1 Oct. 2013. https://rip.trb.org/view/1268074
[28] Structural Health Monitoring and Remote Sensing of Transportation Infrastructure Using Embedded Frequency Selective Surfaces. [Project]. Research and Innovative Technology Administration, Missouri University of Science and Technology, Rolla. Start date: 1 Aug. 2013. https://rip.trb.org/view/1316138
[29] Robotic Inspection of Bridges Using Impact-Echo Technology. [Project]. University Transportation Research Center. Start date: 1 Oct. 2012. https://rip.trb.org/view/1262508
[30] Nondestructive Evaluation of MoDOT Bridge Decks - Pilot Study. [Project]. Missouri Department of Transportation. Start date: 30 Aug. 2012. https://rip.trb.org/view/1301303
[31] Integrated Remote Sensing and Visualization (IRSV) System for Transportation-Infrastructure Operations and Management Phase II. [Project]. Research and Innovative Technology Administration. Start date: 4 Jan. 2010. https://rip.trb.org/view/1263737
[32] Development of an ML-based Georgia Pavement Structural Condition Evaluation System. [Project]. Georgia Department of Transportation. Start date: 22 Jan. 2024. https://rip.trb.org/view/2340092
[33] Asset Management of Bridges Using Uncrewed Aerial Vehicles and Machine Learning Models. [Project]. Office of the Assistant Secretary for Research and Technology. Start date: 1 Sep. 2023. https://rip.trb.org/view/2244357

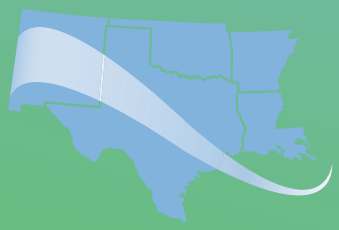

SOUTHERN PLAINS
TRANSPORTATION CENTER

The University of Oklahoma | OU Gallogly College of Engineering
202 W Boyd St, Room 213A, Norman, OK 73019 | (405) 325-4682 | Email: sptc@ou.edu